Dimethyl carbonate synthesis *via* transesterification of propylene carbonate with methanol by ceria-zinc catalysts: Role of catalyst support and reaction parameters

Praveen Kumar, Vimal Chandra Srivastava[†], and Indra Mani Mishra

Department of Chemical Engineering, Indian Institute of Technology Roorkee, Roorkee 247667, Uttarakhand, India

Abstract−Ceria and zinc oxide catalyst were impregnated onto various oxide supports, namely Al_2O_3, TiO_2 and SiO_2, individually by deposition-coprecipitation method. The synthesized catalysts (CZA, CZS and CZT having supports Al_2O_3, TiO_2 and SiO_2, respectively) were characterized by X-ray diffraction (XRD), NH_3- and CO_2-temperature programmed desorption (TPD) and N_2 adsorption. These catalysts were used for synthesis of dimethyl carbonate (DMC) from methanol and propylene carbonate in a batch reactor. CZS was found to have larger average grain size as compared to CZA and CZT. Composite oxides (catalysts) were found to contain individual phases of ZnO, CeO_2 and some spinel forms of Zn, Ce along with their supports. CZS having highest basicity and surface area showed better catalytic activity as compared to CZA and CZT. Effect of reaction temperature and methanol/PC molar ratio on DMC yield was studied and a reaction mechanism has been discussed. Maximum DMC yield of 77% was observed with CZS catalyst at 170 $^\circ$C with methanol/PC molar ratio of 10.

Keywords: DMC, Transesterification Catalysts, Propylene Carbonate, Methanol
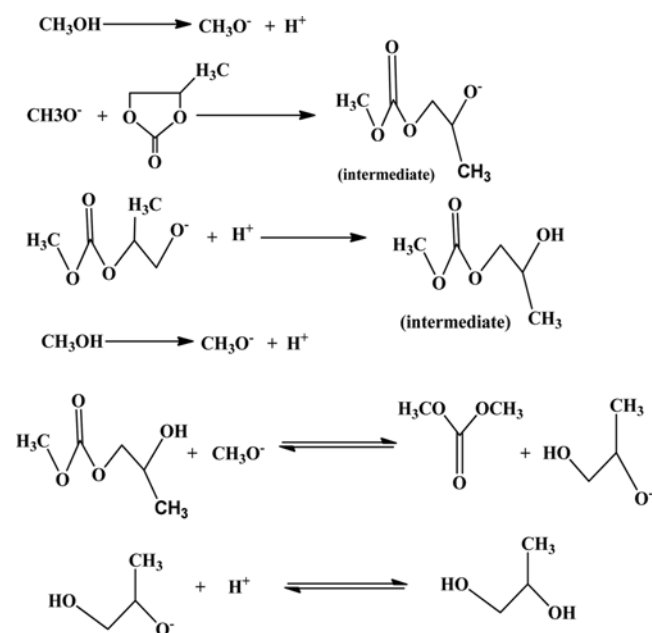
INTRODUCTION

Dimethyl carbonate (DMC) is an environmentally benign building block chemical compound that has diversified uses in the chemical industry [1]. It has low eco-toxicity, and low persistence and bioaccumulation in life forms [2,3]. DMC is a non-toxic chemical widely used as a methylation agent for substituting the highly toxic dimethyl sulfate and dimethyl halides, and also as a carbonylation agent in various applications [1-3]. The high dielectric constant of DMC allows it to be used as an electrolyte too. It is also used in electrolytic lithium batteries [3]. DMC is used in the production of glycerol carbonate [4,5], O-methylation [6], diphenyl carbonate [7], and can be used as a substitute in place of many conventional solvents [4-8].

DMC is also an alternative oxygenate additive in gasoline-based fuels in place of toxic and poorly biodegradable methyl tert-butyl ether (MTBE). It has higher oxygen content on weight basis (53.3%) in comparison to methanol (50%), ethanol (34.89%) and MTBE (17.6%). The use of DMC in gasoline also reduces the emission of solid particulates (SPM) and NOx [1-3].

Traditionally, DMC was produced by using the phosgenation process, methanol oxycarbonylation process and methyl nitrite carbonylation process. Phosgenation of methanol was considered to be hazardous, and therefore, this process of DMC production was abandoned by 1980. Currently, DMC is predominantly produced from methanol oxycarbonylation process [1-3]. These conventional DMC production processes are not considered to be safe, as they suffer from problems such as the production of carbon monoxide, hydrogen chloride and nitric oxide through the complex reaction pathways [1-3]. Some other pathways used for the production of DMC such as the direct synthesis from CO_2 suffer from low conversion to DMC, and has thermodynamic limitations [9-12]. Urea methanolysis process suffers from low selectivity because of the formation of the byproducts such as methyl carbamate, N-methyl urea, N-methyl methyl carbamate [13-15]. Transesterification of propylene carbonate (PC) with methanol is a promising method for the synthesis of DMC. The catalytic mechanism for transesterification

Scheme 1. Proposed reaction mechanism of DMC synthesis.

[†]To whom correspondence should be addressed.
E-mail: vimalcsr@yahoo.co.in, vimalfch@iitr.ac.in

of PC with methanol is shown in Scheme 1. PC gets easily converted to DMC in the presence of a catalyst, but the reaction is reversible and propylene glycol (PG) is formed as byproduct [15]. In this reaction, yield of DMC is higher than other routes. Also, the number of byproducts is less; therefore, separation of products and raw materials is easy and economical as compared to other routes of DMC formation. Although each production method has its own drawback, transesterification of PC with methanol is a promising and feasible method for the synthesis of DMC, especially in the framework of green chemistry, and is environmentally benign as compared to other routes. This route is sustainable, clean, and there is no formation of any harmful or waste byproduct [15].

Ceria-zinc oxide based catalysts have been used in CO oxidation, steam reforming, methanolysis, desulfurization, etc. as shown in Table S1. Comparative assessment of the characterization of ceria-zinc based catalysts and their applications are given in Table S1. It can be seen that the ceria-zinc oxide supported on $Al_2O_3/SiO_2/TiO_2$ has never been used for the synthesis of DMC using transesterification reaction. Most of the researchers also did not characterize the ceria-zinc catalyst.

Various catalysts have been investigated for the synthesis of DMC from PC and methanol such as ion exchange resins [16], pure metal oxide [17], basic ionic liquids [18], mixed metal oxide [19] and double metal cyanide [20]. Comparative performance of various catalysts used for the synthesis of DMC using transesterification of PC is given in Table 1 [20-24]. Srivastava et al. [20] reported that the double metal cyanide catalysts used for the synthesis of DMC gave 87.7% yield after 8 h reaction time. Jeong et al. [21] reported 54.1% conversion and 86.5% selectivity after 6 h with methanol to PC ratio 8 : 1. Wang et al. [22] reported 55% conversion of PC using the CaO-ZrO_2 catalyst after 2 h of reaction with a methanol to PC ratio of 6 : 1. Liu et al. [23] using Na-ZrO_2 catalysts, reported 50% conversion of PC after 1.5 h with a methanol to PC ratio of 5 : 1. Unikrishnan and Srinivas [24] reported 65.4% PC conversion using hydrotalcite based catalyst for the synthesis of DMC from methanol and PC (with 10 : 1 ratio) in 2 h time. To the best of our knowledge, transesterification of PC with methanol in the presence of ceria-zinc oxide catalyst supported on $Al_2O_3/SiO_2/TiO_2$ has not been reported to date.

In this work, a series of cerium-zinc composite oxide catalysts were synthesized using the deposition-coprecipitation method and characterized using X-ray diffraction (XRD), N_2-sorption and Fourier transform infrared spectroscopy (FTIR) techniques. Basicity and acidity of the synthesized catalysts were determined by CO_2- and NH_3-temperature-programmed desorption (TPD), morphology of catalysts was studied using scanning electron microscopy (SEM), transmission electron microscopy (TEM) and atomic force microscopy (AFM). The catalysts were then tested for the production of DMC using transesterification of PC with methanol.

EXPERIMENTS

1. Materials

Zinc nitrate hexahydrate ($Zn(NO_3)_2 \cdot 6H_2O$), cerium nitrate hexahydrate ($Ce(NO_3)_3 \cdot 6H_2O$) and DMC were purchased from Himedia Chemicals, India; Al_2O_3 and TiO_2 were kindly supplied by Evonik Degussa Gmbh; SiO_2 from Thomas Baker; ammonia solution and methanol from Renkem, India. Standard samples of DMC, PC and PG were purchased from Aldrich, India. Only analytical grade (AR) chemicals were purchased and used as required. Double distilled water was used in the synthesis of the catalyst, washing, etc.

2. Catalyst Preparation

Ceria and zinc oxide were impregnated onto various oxide supports, namely Al_2O_3, TiO_2 and SiO_2. These catalysts were synthesized in the $CeO_2 : ZnO : support = 1 : 1 : 2$ molar ratio by a deposition-coprecipitation method using liquid ammonia as the precipitating agent. Metal precursors such as hexahydrates of cerium nitrate and zinc nitrate were dissolved separately in double distilled water with a 1 : 1 molar ratio and mixed together at room temperature. The supporting oxide was dispersed in water, stirred vigorously and thereafter metal precursor cerium-zinc solutions were mixed together [25]. The prepared mixture was diluted with 100 mL of double distilled water and stirred for 1 h. Liquid ammonia was added drop by drop in the mixture under vigorous stirring until the pH reached 8.5. The obtained precipitate was filtered and washed with double distilled water until it was free from all anion impurities. Thereafter, the solid precipitate was dried at 110 °C for 24 h and calcined at 500 °C under air atmosphere for 4 h. The composite oxides, thus formed, were denoted as CZA, CZT and CZS, where C, Z, A, T and S denote Ce, Zn, Al, Ti, and Si, respectively.

3. Catalyst Characterization

The metal content was quantified by energy disperse X-ray (EDX) analysis using field emission scanning electron microscope (FE-SEM) (quanta 200 FEG, FEI Netherlands) and a special attachment

Table 1. Comparative study of catalysts with different reaction conditions

Catalyst	Methanol: PC ratio	Amount of catalyst (wt%)	Reaction time (h)	Reaction temp. (°C)	PC conversion (%)	Selectivity (%)	Yield (%)	Reference
Fe-Zn cyanide	10 : 1	5.75	8	170	-	-	87.7	[20]
CaO-ZrO_2	6 : 1	1.5	2	150	55	-	-	[22]
Na-ZrO_2	10 : 1	1.5	1.5	160	50	-	-	[23]
Mg-Al-La	10 : 1	5.0	2	150	65.4	87.7		[24]
CZA	10 : 1	1.0	6	170	-	-	68	This work
CZS	10 : 1	1.0	6	170	-	-	77	This work
CZT	10 : 1	1.0	6	170	-	-	23	This work

PC: Propylene carbonate

of electron backscatter diffraction (EDBS) equipped with an analysis software. The estimates of the metal content by this method may have an error of ±5%. TEM images were obtained by using TECNAI G^2 20S-TWIN, FEI, Netherlands at 200 kV. For TEM analysis, the catalysts were dispersed in ethanol solution, which was sonicated for 60 min. Afterwards, a drop of the dispersion was placed on a TEM copper grid.

Morphology of the catalysts was also studied using AFM supplied by M/s Molecular Tools and Devices for Nanotechnology (NT-MDT) which was equipped with NOVA software for image analysis. The samples were prepared in ethanol; a small amount of sample dispersed in ethanol solution, which was sonicated for 120 min. Afterwards, a small amount of solution dispersion was placed on a glass plate and dried at room temperature for 12 h. Then this glass plate was used for AFM analysis.

Thermo-gravimetric analysis (TGA) of the synthesized catalysts was carried out using SII 6300 EXSTAR analyzer. The weight loss was estimated from room temperature to 1,000 $^{\circ}$C with heating rate of 10 K/min under flushing nitrogen atmosphere.

FTIR spectroscopy was used to find the surface functional groups of the synthesized catalysts by using an FTIR spectrophotometer (Thermo Nicolet, Model Magna 760) in the wave number range of 400-4,000 cm^{-1} using a hand pressed KBr pellet as the reference material.

Various analytical methods were used for characterizing the morphology, phase structure, and physical properties of the prepared catalysts. XRD patterns of the catalyst surface were obtained from an X-ray diffractometer (Brueker AXS, Diffractomer D8, Germany) with Cu-K$_\alpha$ radiation (λ=1.5406 Å) and X-ray gun operated at 40 kV and 30 mA. The scanning of the catalysts was done in the 2θ range of 5°≤2θ≤100°. XRD line positions were found with a step size of 0.02°. The crystallinity of the sample was identified by using ICDD-JCPDS data base. Crystal size (L) was calculated from the Scherrer equation.

$$L = \frac{K \cdot \lambda}{\beta \cos\theta} \tag{3}$$

where, K is the Scherrer's constant (generally taken as 0.9), λ is the wavelength of X-ray radiation and is equal to 1.5405 Å, β is the full width of the reflection at half maximum (FWHM) in radians and θ is the scattering angle of the main reflection.

The textural properties of the catalysts were determined by using multi-point N$_2$ adsorption-desorption at −195 $^{\circ}$C using a Micromeritics ASAP 2020 instrument. The sample was kept overnight at 110 $^{\circ}$C and then degassed for 12 h at 200 $^{\circ}$C under high vacuum. Data of N$_2$ adsorbed at different relative pressures were analyzed by Brunauer-Emmett-Teller (BET) [26] and Barrett-Joyner-Halenda (BJH) [27] isotherm equations to determine various textural properties.

NH$_3$- and CO$_2$-TPD was performed using Micromeritics Chemi-Sorb 2720 instrument fitted with a thermal conductivity detector (TCD). The 50 mg sample was first degassed under helium flow (25 mL/min) in a quartz U-tube at 200 $^{\circ}$C for 4 h, and then allowed to cool to room temperature under flowing helium. The NH$_3$ adsorption was performed by admitting 10% NH$_3$/He stream flow (25 mL/min) at 50 $^{\circ}$C up to saturation. Subsequently, the sample was exposed to a flow of helium (25 mL/min) at 50 $^{\circ}$C for 2 h to

remove any physically bound ammonia from the surface. Desorption study was carried out in the temperature range of 50-900 $^{\circ}$C at a heating rate of 10 K/min under helium flow (20 mL/min). CO$_2$-TPD followed the NH$_3$-TPD procedure. The acidity and basicity of the synthesized catalysts were calculated from NH$_3$-TPD and CO$_2$-TPD peak areas using calibration curves. Joe et al. [13] activated the CeO$_2$-ZnO catalysts at 500 $^{\circ}$C and studied the TPD profile in the temperature range of 0-900 $^{\circ}$C. Similarly, He et al. [28] used calcination temperature of 750 $^{\circ}$C for CeO$_2$/ZnO nanostructured microsphere activation and studied the CO$_2$-TPD profile in the temperature range between 0-800 $^{\circ}$C. On the basis of these studies, in the present study, TPD in the present study was analyzed in the temperature range of 0-1,000 $^{\circ}$C.

4. Reaction Procedure

Synthesized catalysts were tested for their activity to produce DMC through transesterification of PC with methanol. Experiments were performed in a 300 mL steel autoclave (Parr, model 4843). 0.25 mol of PC along with 2.5 mol of methanol and a known mass of the synthesized catalyst (about 1.0 wt% of the PC) were placed in the steel autoclave. The autoclave was flushed with nitrogen under continuous heating and stirring at 550±50 rpm so as to increase the autoclave pressure to 2-5 bar. The reactions were carried out at 170 $^{\circ}$C and autogenic pressure up to 25 bar for 4 h. After the desired time, the reaction was stopped and the product mixture was cooled to 10 $^{\circ}$C with the help of cold water and ice for 30 min. After that the catalyst was separated by centrifugation/filtration. The reaction products were analyzed by gas chromatograph (Thermo Electron Corporation, model Trace GC ultra) equipped with flame ionization detector (FID) with HP-5 capillary column. The initial column temperature was 40 $^{\circ}$C with a hold time of 5 min, after which it was increased at a rate of 3 K/min to 90 $^{\circ}$C with a hold time of 2 min. Temperature was further increased at a rate of 10 K/min to final temperature of 270 $^{\circ}$C where the hold time was 2 min. Injector and detector temperatures were 250 and 270 $^{\circ}$C, respectively, with nitrogen gas used as the carrier gas.

RESULTS AND DISCUSSION

1. Catalyst Characterization
1-1. Morphological, Functional and Structural Properties

SEM and TEM images of the synthesized CZA, CZS and CZT catalysts are shown in Fig. 1. All the catalysts show spherical morphology, heterogeneous and crystalline structure. The EDX image mapping of CZA, CZS and CZT catalysts is shown in Fig. S1. The image maps show the distribution of Al, Si and Ti metals in CZA, CZS and CZT catalysts. In the CZA, the element Al is most scattered in CZA. Ti is well distributed and has least aggregation in CZT. EDX mapping also shows an almost even distribution of Ce and Zn in all catalysts. Average particle size of the catalysts as determined from the FE-SEM studies is found to be in the range of 5-20 nm. TEM image show that all particles are in the diameter range of ≈5-10 nm. AFM 3D images along with grain size distribution of the CZA, CZS and CZT is given in Fig. 2. Average grain size (as estimated using AFM image) of CZA, CZS and CZT was found to 5.25 nm, 8.65 nm and 4.10 nm, respectively. Thus, CZS was found to have larger average grain size as compared to CZA and CZT.
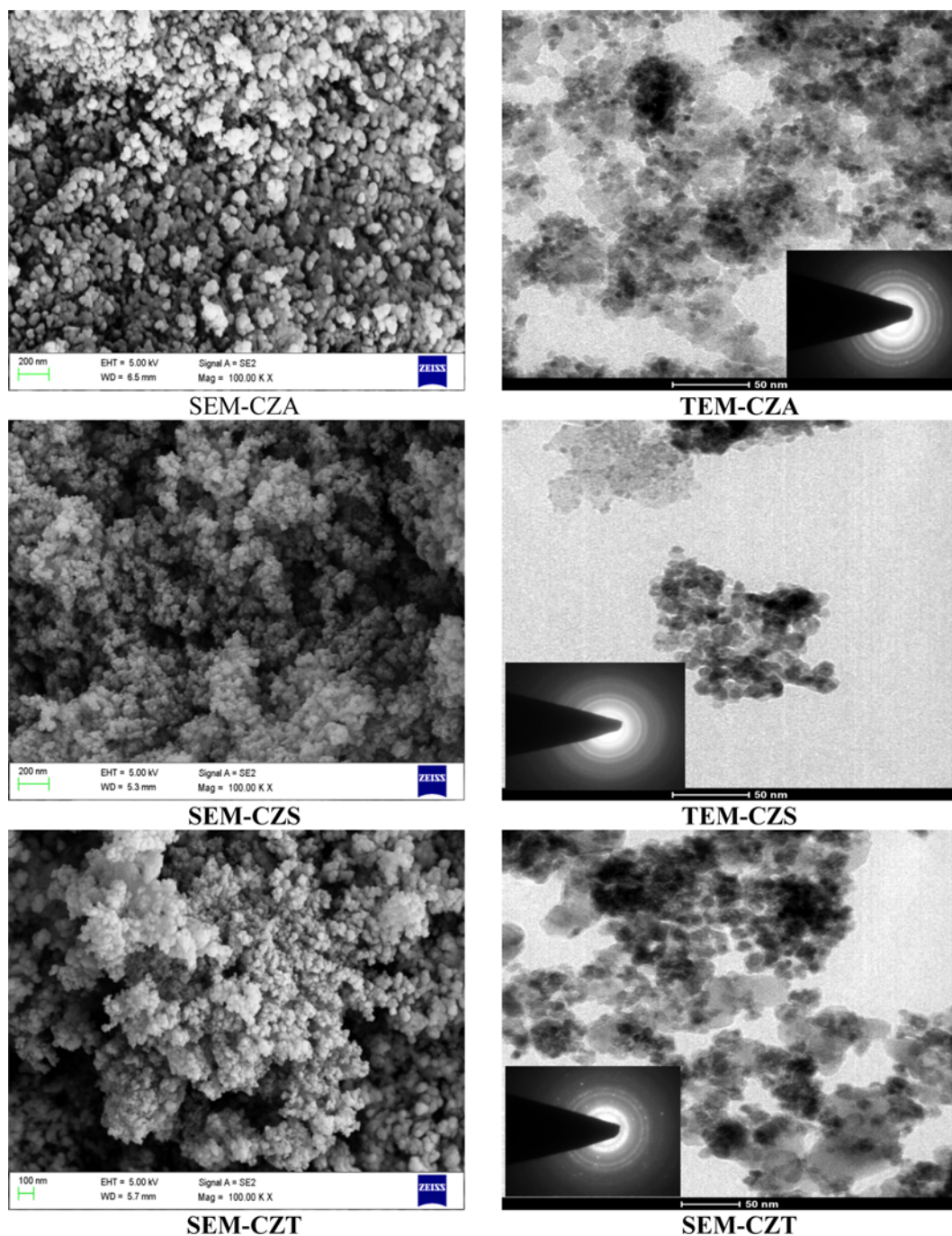
Fig. 1. SEM and TEM of CAZ, CZS and CZT catalyst.

FTIR spectra of CZA, CZS and CZT catalysts are shown in Fig. 3. The origin of the vibration band seen at ~3,430 cm^{-1} can be ascribed to surface O-H stretching, absorbed water and N-H stretching amines groups. The peak at ~2,925 cm^{-1} in all the catalysts is due to C-H stretching and the peak at ~1,630 cm^{-1} is due to N-H bending. In CZA catalyst, the vibrations appearing in the peak at 735 cm^{-1} are due to Al-O vibrations and that at 543 cm^{-1} is due to Zn-O vibrations [29,30]. The characteristic vibration band for Si-O-Si of the [SiO$_4$] tetrahedron vibration unit in CZS is observed at ~1,100 cm^{-1}. The peaks at 463 and 805 cm^{-1} correspond to the ZnO and O-Si-O group, respectively [31].

XRD patterns of CZA, CZS, and CZT catalysts are shown in Fig. 4. The XRD peaks for CZA are found at 2θ angles of 28.629^o, 33.042^o, 47.577^o and 56.545^o corresponding to (111), (200), (220) and (311) planes, respectively, and representing face centered cubic lattice. The XRD pattern of CZA indicates the presence of CeO$_2$ (PDF-ICDD 001-0800), Al$_2$O$_3$ (PDF-ICDD 004-00879), ZnO (PDF-ICDD 003-0888) and spinel form of CeAlO$_3$ (PDF-ICDD 021-0175). The XRD peaks for CZS are found at 2θ angles of 28.804^o, 33.267^o, 47.451^o and 56.594^o corresponding to (111), (002), (022) and (113) planes,
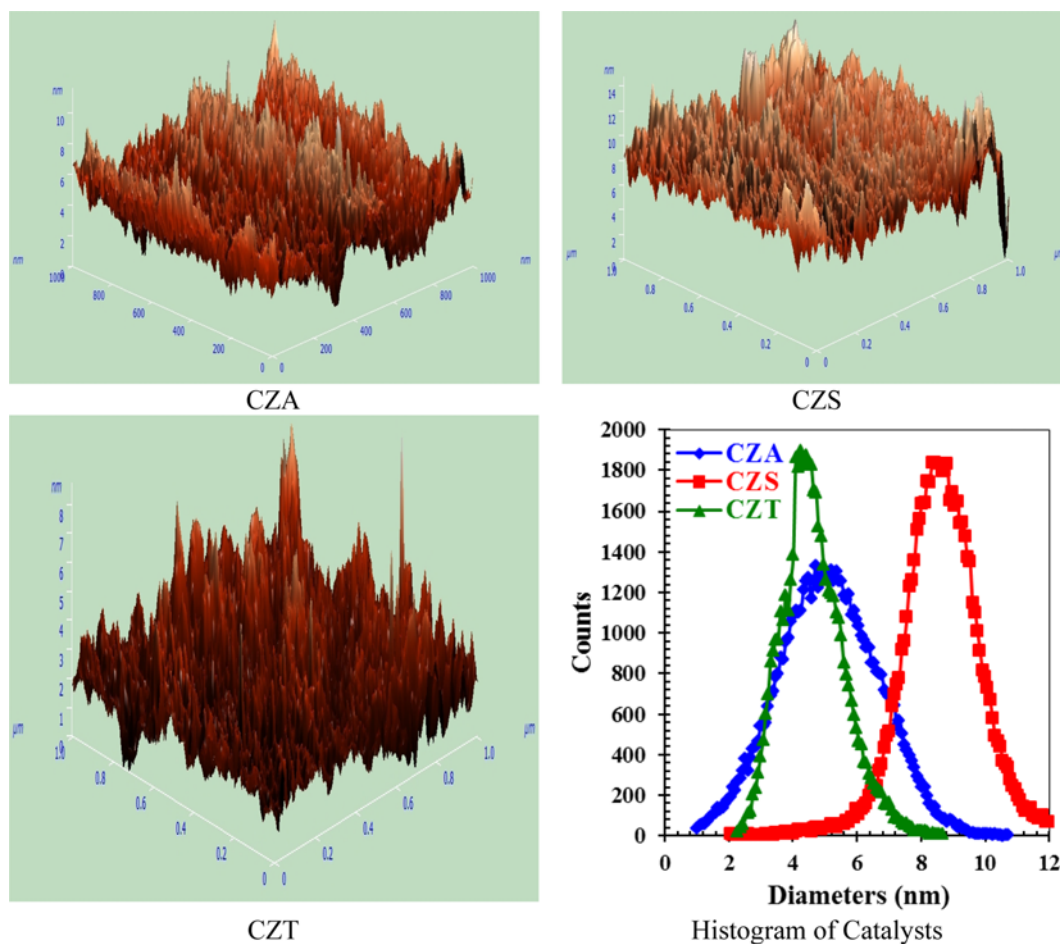
Fig. 2. 3D AFM - image and histogram of CZA, CZS and CZT catalysts.
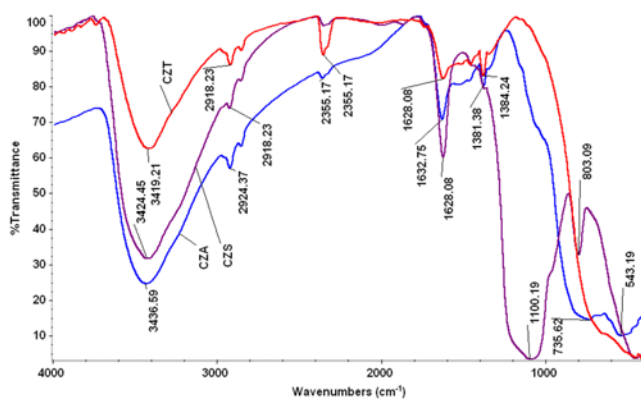

Fig. 3. FTIR spectra of CZA, CZS and CZT catalysts.

respectively, and representing face centered cubic lattice. These peaks indicates presence of ZnO (PDF-ICDD 00-003-0752), CeO_2 (PDF-ICDD 00-002-1306), SiO_2 (PDF-ICDD 008-0018), $Ce_2Si_2O_7$ (PDF-ICDD 048-1588) and Zn_2SiO_4 (PDF-ICDD 002-0813) in CZS. The XRD peaks for CZT catalyst are seen at 2θ angle of 25.227^o, 28.569^o, 33.165^o, 47.894^o, and 56.58^o corresponding to (111), (200), (210), (311) and (330) plane, respectively. CeO_2 (PDF-ICDD 001-0800), ZnO (PDF-ICDD 003-0752), TiO_2 (PDF-ICDD 001-0562) and Zn_4TiO_6
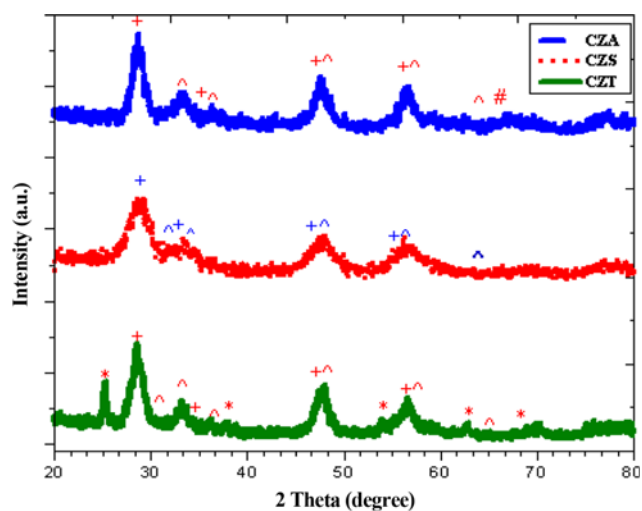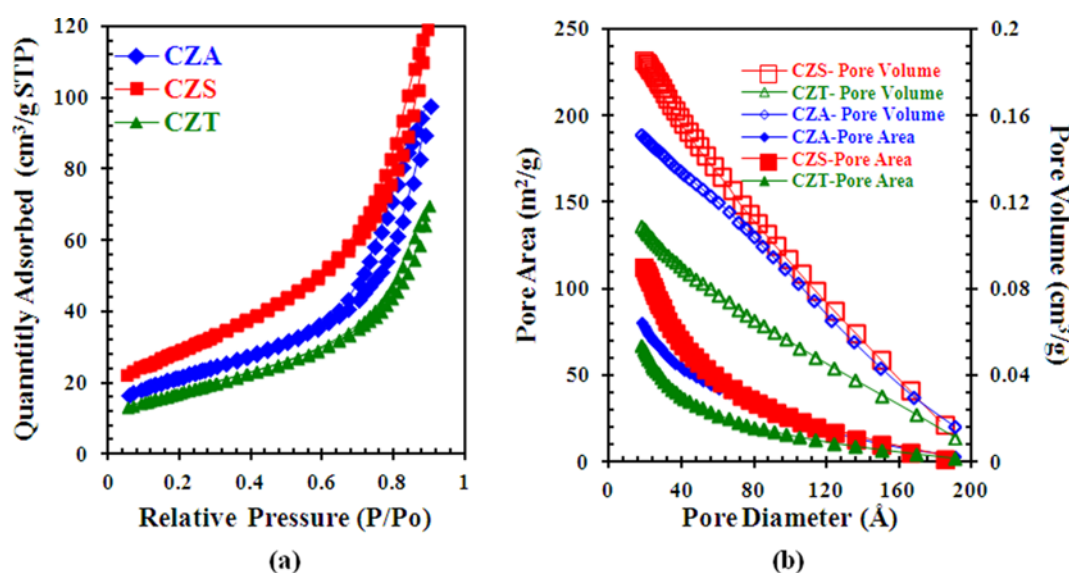

Fig. 4. XRD patterns of CZA, CZS, and CZT catalysts at 500 °C. (+) Lines due to CeO_2; (^) lines due to ZnO; (#) lines due to γ-Al_2O_3; (*) lines due to TiO_2 anatase.

(PDF-ICDD 049-0687) are found to be present on CZT [32,33]. All the CZA, CZS and CZT catalysts exhibited the mixed peaks of ZnO and CeO_2 phases. Fig. 4 also shows that the individual peak

Table 2. Crystallite size and textural properties of CZA, CZS and CZT catalysts

Catalyst	XRD			Textural properties			Maximum yield (%)
	Unit cell parameter (Å)[a]	Crystallite size (nm)[a]	Structure[a]	Surface area (m²/g)	Pore volume (cm³/g)[b]	Average pore diameter (nm)[c]	
CZA	5.42	3.70	Cubic	77	0.150	7.5	68
CZS	6.29	3.90	Cubic	104	0.187	6.3	77
CZT	5.38	3.05	Cubic	61	0.108	6.4	23

[a]The unit cell parameter, crystal size and structure is calculate using XRD
[b]BJH desorption cumulative pore volume of pores in the range 17 to 3,000 Å
[c]BJH desorption average pore diameter

Fig. 5. (a) Adsorption/desorption isotherms of N₂ at 77 K; (b) pore size distribution for CZA, CZS and CZT catalysts.

positions for CeO₂ and ZnO remain intact in the composite oxides. This is an indication that the composite oxides contain individual phases of ZnO, CeO₂ and some spinel forms of Zn, Ce with their supports. The CeO₂ peaks for catalysts CZA, CZS and CZT have been used in Scherrer's equation to calculate the crystallite size of ceria using X-ray line broadening analysis. The data is summarized in Table 2. It is observed that the γ-Al₂O₃, SiO₂ and TiO₂ affect the particle size of ceria.

1-2. Textural Properties

The BET surface area, pore size distribution and pore volume as obtained from the corresponding instruments are given in Fig. 5 and Table 2. The synthesized catalysts have surface area in the range of 61-104 m²/g. The adsorption–desorption isotherms of the catalysts at 77.2 K confirm the generation of mesopores during their synthesis and the absence of micropores as shown in Fig. 5. All the adsorption-desorption isotherms are of type III, according to the IUPAC interpretation and exhibit an H3 hysteresis loop [34,35]. This confirms the presence of mesopores and absence of micropores in the synthesized catalysts. If the relative pressure increases (P/P$_o$>0.60), then the isotherms show the capillary condensation of nitrogen within the uniform mesopores, where the P/P$_o$ position of the influence points is related to the diameter of the mesopores [36]. Among silica, alumina and titania supports, the specific

surface is as follows: silica>alumina>titania [37]. Therefore, metal oxides impregnated on these supports also follow the same trend. Borgmann and Wedler [38] have reported similar trend of BET surface area for cobalt supported impregnated silica, aluminum and titania catalysts. Reddy et al. [25] also observed similar BET surface area trend for aluminum, silica and titania supported ceria-zirconia catalyst.

The fractal dimension, often used as an index for estimating the irregularity or roughness of the catalyst surface, was studied using the Frenkel-Halsey-Hill (FHH) equation [39] for the CZA, CZS and CZT catalysts, to the adsorption isotherm of N₂ [40]:

$$\frac{q}{q_e} = K \ln\left(\frac{P_o}{P}\right)^{D-3} \qquad (2)$$

where, q is the amount adsorbed at equilibrium pressure P, P$_o$ is the saturated pressure, D is the fractal dimension, q$_e$ is the amount adsorbed filling micropore volume and K is a constant. The logarithmic plot of (q/q$_e$) versus (P$_o$/P) showed linear behavior, and D was calculated from the slope (D−3) of the straight line. Surface smoothness, irregular nature or roughness depends upon the D value. If D=2, then the surface is considered to be perfectly smooth, whereas if D=3, then the surface is very irregular or very rough. For the synthesized catalysts, the fractal dimension was found to
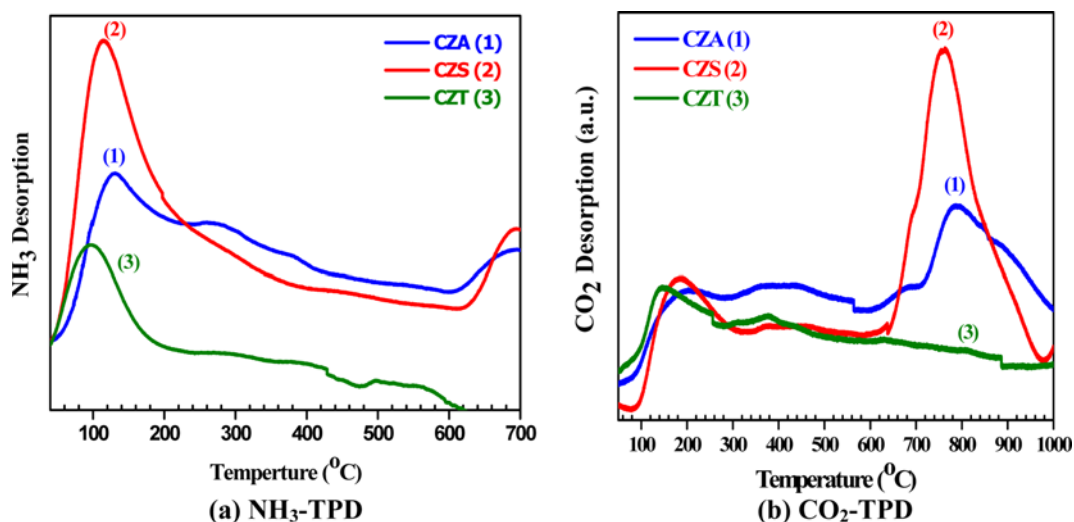
Fig. 6. TPD profile of synthesized catalysts.

Table 3. TPD analysis using absorbed NH_3 and CO_2 for determining acidic and basic properties of synthesized catalysts

Catalyst	TPD analysis of absorbed NH_3 (mmol/g)			Total NH_3 evolved (mmol/g)	Acid site density (μmol/m²)
	Weak (<200 °C)	Moderate (200-450 °C)	Strong (>450 °C)		
CZA	0.691 (131)	0.116 (282)		0.807	10.48
CZS	1.288 (113)	-		1.288	12.38
CZT	0.343 (99)	0.001 (296)		0.344	5.64

Catalyst	TPD analysis of absorbed CO_2 (mmol/g)			Total CO_2 evolved (mmol/g)	Basic site density (μmol/m²)
	Weak (<200 °C)	Moderate (200-450 °C)	Strong (>450 °C)		
CZA	0.242 (177)	-	0.795 (796)	1.037	13.47
CZS	0.719 (188)	0.151 (459)	1.951 (763)	2.821	27.12
CZT	0.713 (145)	-	-	0.713	11.69

Temperature (°C) at maxima is given in brackets

be 2.514 for CZA, 2.441 for CZS and 2.511 for CZT. This shows the similarity of the surface heterogeneity among the synthesis catalysts, with a maximum deviation of 3%.

1-3. NH_3-TPD

To investigate the acid properties for the synthesized cerium-zinc with different supported catalysts, NH_3-TPD analysis was performed [41]. NH_3 desorption is temperature-dependent and can be classified in three stages: as weak (<200 °C), moderate (200-450 °C) and strong (>450 °C). Profiles of NH_3-TPD on the supported Ce-Zn catalysts are shown in Fig. 6(a), and the acidity of catalysts calculated from NH_3-TPD peak area is summarized in Table 3. Two NH_3 desorption peaks at 131 °C and 282 °C were observed for CZA. Intensity of the peak is 0.691 mmol/g at 131 °C and 0.116 mmol/g at 282 °C. These peaks could be ascribed to the desorption of NH_3 from weak and moderate Lewis acid sites, respectively. CZS catalyst showed NH_3 desorption peaks at 113 °C with 1.288 mmol/g intensity corresponding to weak Lewis acid site only. CZT catalyst showed the NH_3 desorption peaks at 99 °C with an intensity of 0.344 mmol/g in the weak region only. According to NH_3-TPD results, the total acidity of the synthesized CZA, CZS and CZT catalysts was 0.807 mmol/g, 1.288 mmol/g and 0.344 mmol/g, respectively.

1-4. CO_2-TPD

The profiles of CO_2-TPD of the synthesized Ce-Zn with supported catalysts are shown in Fig. 6(b) and the basicity of the catalysts calculated form CO_2-TPD peak area is summarized in Table 3. The CO_2-TPD can be classified as weak (<200 °C), moderate (200-450 °C) and strong (>450 °C). CZT catalyst showed only weak basicity observed by peak around 145 °C. CZA catalyst shows two distinct peaks at 242 °C and 796 °C in the moderate and strong region, respectively. For CZS catalyst, peaks are observed in all the three regions at 188, 459 and 763 °C. According to the CO_2-TPD results, CZS catalyst showed strong, moderate, and weak basic sites, with intensities of 1.951 mmol/g, 0.151 mmol/g and 0.719 mmol/g, respectively, and the total basic amount being 2.821 mmol/g. CZA showed desorption behavior at strong (>450 °C) and weak basic sites (<200 °C) with the basic amount being 0.795 mmol/g and 0.242 mmol/g, respectively. CZT catalyst showed only weak basic sites with intensity of 0.823 mmol/g.

Silanol groups in amorphous silica provide weak Brønsted acidity. Calcination of silica increases the Lewis acidity and basicity due to activation of siloxane groups by dehydration reaction. In comparison, alumina and titania supports develop lower amount

of Lewis acidity and basicity during their calcination [35]. Synthesized Ce-Zn have both acidic and basic sites, indicating that the catalysts can act as acid-base bifunctional catalysts; however, support materials varied the nature of the catalysts. A few investigators have reported that the presence of both acidic and basic sites helps in the transesterification of PC with methanol used for DMC synthesis [17,20].

1-5. Thermal Stability

Thermal stability of the synthesized catalysts was determined by thermogravimetric analysis. TGA, differential thermal gravimetry (DTG), differential thermal analysis (DTA) traces of the CZA, CZS and CZT catalysts are shown in Fig. S2. TGA traces show mass loss of 7.3%, 8.03% and 4.4% for CZA, CZS and CZT catalysts, respectively, in the temperature range of 20-200 °C. These mass losses may be due to vaporization of low boiling point organic molecules including moisture. Mass loss of 8% for CZA, 8.3% for CZS and 6.9% for CZT was observed in the range of 200-500 °C. At 1,000 °C, the catalyst samples retained residual mass of 84.7%, 83.7% and 88.7% of the original mass for CZA, CZS and CZT catalysts, respectively. Thus, all the catalysts were highly thermally stable.

2. Catalytic Activity for DMC Synthesis

The catalytic activity of the cerium-zinc oxide stabilized on the three supports was tested for the transesterification of PC with methanol. The activity measurement was performed at the initial pressure of 2-5 bar and the final pressure of 20-25 bar. One mol of PC reacts with two moles of methanol to produce one mole of DMC and one mole of PG. However, an excess amount of methanol drives the reaction towards the transesterified product.

The effect of temperature on the synthesis of DMC was investigated over the temperature range of 120-200 °C. The results are shown in Fig. 7(a). Maximum DMC yield of 77% was obtained at 170 °C for CZS catalyst, whereas CZA and CZT gave 68% and 23% DMC yield, respectively at 170 °C. The DMC yield increases with an increase in temperature up to 170 °C and, thereafter decreases with an increase in the reaction temperature. At all temperatures more

than 170 °C, side reactions and/or decomposition of DMC to PC and formation of the byproduct PG are observed. The optimum synthesis temperature for DMC was 170 °C, giving an optimum yield of 77% with CZS catalyst. The optimum reaction temperature for transesterification of PC with methanol for DMC synthesis were reported to be 160 °C by Wang et al. [22] and Wei et al. [17]. Srivastava et al. [20] reported 170 °C as the optimum temperature.

The effect of molar ratio of methanol/PC on the synthesis of DMC using the three catalysts is shown in Fig. 7(b). It is found that the DMC yield increases with an increases the mole ratio of methanol/ PC. Maximum DMC yield is observed at a methanol/PC molar ratio of 10 for all the catalysts. When the molar ratio of methanol/PC is lower, the side reaction forming PG takes place, thereby adversely affecting the DMC formation. Higher methanol/PC ratio shifts the equilibrium towards the product side [40]. The DMC yield reaches a maximum of 77%, 69% and 23% for CZS, CZA and CZT, respectively, for the molar ratio of 10 for methanol/PC. Srivastava et al. [20] Unnikrishnan and Srinivas [24] Murugan et al. [42] and Kumar et al. [43] reported a methanol/PC molar ratio of 10 as the optimum ratio for the transesterification PC with methanol for the synthesis of DMC using Fe-Zn double-metal cyanide, earth promoted Mg-Al hydrotelcite and KF/Al$_2$O$_3$ catalysts, respectively.

A possible mechanism for the synthesis of DMC from PC with methanol is represented in Scheme 1 [17,44]. Methanol gets activated in the presence of the catalysts to form H$^+$ and CH$_3$O$^-$; CH$_3$O$^-$ attracts the carbonyl C of the PC and forms CH$_3$O-CO-O-CH$_2$-CH(CH$_3$)-O$^-$ as an intermediate, which further reacts with H$^+$ to form an intermediate, CH$_3$O-CO-O-CH$_2$-CH(CH$_3$)-OH (2-methyl-hydroxyethyl methyl carbonate). This intermediate further reacts with CH$_3$O$^-$ to form DMC and intermediate, OH-CH$_3$-CH$_2$-CH$_2$-O$^-$ which reacts with H$^+$ to form PG. The overall reaction of PC with methanol for the synthesis of DMC reaction is exothermic [16]. The main function of the solid basic catalyst is its activation with methanol through the abstraction of H$^+$ by the acid site so as to form CH$_3$O$^-$ which reacts with PC to produce DMC. The higher
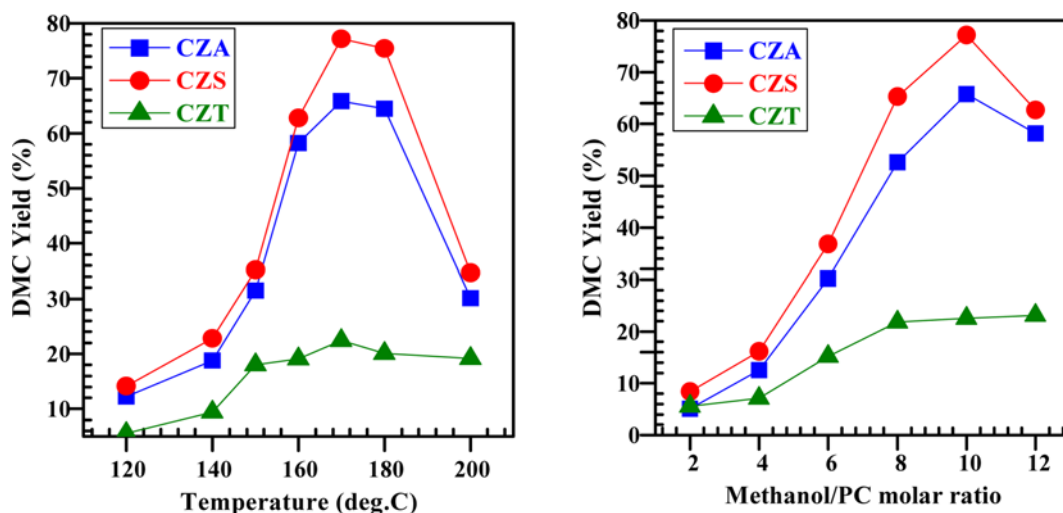

Fig. 7. (a) Effect on reaction temperature on DMC formation using different catalysts; (b) effect on PC to methanol molar ratio on synthesis of DMC using different catalysts at temperature 170 °C (reaction condition: PC=0.25 mol, methanol=2.5 mol, catalyst=5 wt% of reactant, reaction time=4 h).

the basicity of the catalyst, the more negative is the charge of MeO⁻ and lower is the free energy of MeO⁻ with PC.

Overall, CZS catalyst exhibited the best performance as compared to CZA and CZT catalysts. CZS has highest BET surface area, acidic and basic sites per unit mass of the catalyst. Moreover, acid site density (acidic sites per unit surface area) of the synthesized catalysts follow the sequence (Table 3): CZS ($12.38\,\mu mol/m^2$)>CZA ($11.48\,\mu mol/m^2$)>CZT ($5.64\,\mu mol/m^2$). Similarly, the basic site density of the synthesized catalysts has the following sequence (Table 3): CZS ($27.12\,\mu mol/m^2$)>CZA ($13.47\,\mu mol/m^2$)>CZT ($11.69\,\mu mol/m^2$). Thus, the basic and acidic site densities and the catalytic activity followed a similar trend. CZS having higher basicity lowers the free energy of this reaction and enhances the yield of DMC by the transesterification reaction [17].

Juarez et al. [45] used a series of metal oxide nanoparticles namely MgO, ZrO_2, CeO_2 and Au/CeO_2 (1.5 wt%) with acid or basic properties exhibit low to moderate activity towards the transesterification of PC with methanol. They reported that strongly basic MgO increases the PC conversion, however, for PC hydrolysis with very poor selectivity towards DMC. ZrO_2, which is an acid metal oxide, showed low PC with better selectivity towards DMC. CeO_2 exhibited intermediate activity and selectivity towards DMC formation. Yield with CeO_2 was much better than MgO and ZrO_2 (in that order). Gold nanoparticles supported on nanocrystalline ceria (Au/CeO_2) exhibited much higher PC conversion, DMC selectivity and yield than CeO_2. Wang et al. [46] used zinc-yttrium based catalysts for synthesis of DMC via transesterification of ethyl carbonate (EC) with methanol. The yield of the DMC directly correlated well with the BET surface area and basicity of the catalysts. Cui et al. [47] studied synthesis of DMC through the transesterification of EC using MgO and mesoporous silica coated MgO ($MgO-SiO_2$) catalyst. BET surface area of $MgO-SiO_2$ ($412.6\,m^2/g$) was much larger than that of the pure flower-like MgO ($141.4\,m^2/g$). With MgO, EC conversion in the first run was 92%, which dropped sharply to 52% in the second run, because of the stability issues. For $MgO-SiO_2$, EC conversion was constantly over 80% for 10 consecutive runs. Authors did not report basicity so it was not possible to correlate the results with basicity. Xu et al. [48] investigated various CeO_2 based catalysts (with different surface areas and basicity) for transesterification of EC with methanol for DMC synthesis. Catalyst CeO_2-meso-400 ($182\,m^2/g$ and $212\,\mu mol\,CO_2/g$) had high surface area and high basicity as compared to CeO_2-meso-500 ($149\,m^2/g$ and $178\,\mu mol$ CO_2/g) and CeO_2-meso-600 ($108\,m^2/g$ and $141\,\mu mol\,CO_2/g$). The highest activity was observed with CeO_2-meso-400 with DMC yield of 73.3% as compared to CeO_2-meso-500 (63.8%) and CeO_2-meso-600 (57.1%). Therefore, the basicity and BET surface area of the synthesized catalysts play an important role during DMC synthesis by transesterification reactions. The catalytic activity of the supported catalyst depends upon the support. The XRD patterns, CO_2-TPD, SEM and BET surface area provide interesting information about the synthesized catalysts with different supports and used for the transesterification of PC with methanol to produce DMC.

CONCLUSION

Ceria and zinc oxide were impregnated onto various oxides sup-

ports such as alumina (Al_2O_3), silica (SiO_2) and titania (TiO_2) in the molar ratio of 1 : 1 : 2 by deposition-coprecipitation method. Variation of support changed not only the structure and textural properties of the catalyst, but also the basic strength and basic sites of the catalyst. Acidity and basicity of the catalysts directly influence in the transesterification of PC with methanol. The prepared CZA, CZS and CZT catalyst showed good catalytic activity for the synthesis of DMC from methanol and PC. CZS catalysts had higher catalytic activity due to high basic strength and high BET surface area in comparison to CZA and CZT catalysts. Moreover, the basic strength supplied by the SiO_2 also is improving the highest catalytic activity. DMC yield of 77% was observed with CZS catalyst under optimal conditions (temperature=170 °C and methanol/PC molar ratio=1 : 10).

SUPPORTING INFORMATION

Additional information as noted in the text. This information is available via the Internet at http://www.springer.com/chemistry/journal/11814.

REFERENCES

1. N. Keller, G. Rebmann and V. Keller, *J. Mol. Catal. A: Chem.*, **317**, 1 (2010).
2. Y. Ono, *Appl. Catal. A: Gen.*, **155**, 133 (1997).
3. D. Delledonne, F. Rivetti and U. Romano, *Appl. Catal. A: Gen.*, **221**, 241 (2001).
4. P. Lu, H. Wang and K. Hu, *Chem. Eng. J.*, **228**, 147 (2013).
5. M. G. Alvarez, A. Segarra, S. Contreras, J. E. Sueiras, F. Medina and F. Figueras, *Chem. Eng. J.*, **161**, 340 (2010).
6. X. He, Z. Li, K. Su, B. Cheng and J. Ming, *Catal. Commun.*, **33**, 20 (2013).
7. Z. Li, B. Cheng, K. Su, Y. Gu, P. Xi and M. Guo, *J. Mol. Catal. A: Chem.*, **289**, 100 (2008).
8. R. Xia, Z. Li, B. Cheng and K. Su, *Korean J. Chem. Eng.*, **31**, 427 (2014).
9. H. J. Lee, W. Joe and I. K. Song, *Korean J. Chem. Eng.*, **29**, 317 (2012).
10. H. J. Lee, W. Joe, J. C. Jung and I. K. Song, *Korean J. Chem. Eng.*, **29**, 1019 (2012).
11. V. Eta, P. M. Arvela, A. R. Leino, K. Kordàs T. Salmi, D. Y. Murzin and J. P. Mikkola, *Ind. Eng. Chem. Res.*, **49**, 9609 (2010).
12. H. J. Lee, S. Park, I. K. Song and J. C. Jung, *Catal. Lett.*, **141**, 531 (2011).
13. W. Joe, H. J. Lee, U. G. Hong, Y. S. Ahn, C. J. Song, B. J. Kwon and I. K. Song, *J. Ind. Eng. Chem.*, **29**, 1019 (2012).
14. D. Wang, X. Zhang, Y. Gao, F. Xiao, W. Wei and Y. Sun, *Fuel Process. Technol.*, **91**, 1081 (2010).
15. W. Zhao, W. Peng, D. Wang, N. Zhao, J. Li, F. Xiao, W. Wei and Y. Sun, *Catal. Commun.*, **10**, 655 (2009).
16. A. Pyrlik, W. F. Hoelderich, K. Müller, W. Arlt, J. Strautmann and D. Kruse, *Appl. Catal. B: Environ.*, **125**, 486 (2012).
17. T. Wei, M. Wang, W. Wei, Y. Sun and B. Zhong, *Fuel Process. Technol.*, **83**, 175 (2003).
18. Z. Z. Yang, L. N. He, X. Y. Dou and S. Chanfreau, *Tetrahedron Lett.*, **51**, 2931 (2010).

19. H. Wang, M. Wang, W. Zhang, N. Zhao, W. Wei and Y. Sun, *Catal. Today*, **115**, 107 (2006).
20. R. Srivastava, D. Srinivas and P. Ratnasamy, *J. Catal.*, **241**, 34 (2006).
21. E. S. Jeong, K. H. Kim, D. W. Park, S. W. Park and J. W. Lee, *Reac. Kinet. Catal. Lett.*, **86**, 241 (2005).
22. H. Wang, M. Wang, S. Liu, N. Zhao, W. Wei and Y. Sun, *J. Mol. Catal. A: Chem.*, **258**, 308 (2006).
23. S. Liu, S. Huang, L. Guan, J. Li, N. Zhao, W. Wei and Y. Sun, *Micropor. Mater.*, **102**, 304 (2007).
24. P. Unnikrishnan and D. Srinivas, *Ind. Eng. Chem. Res.*, **51**, 6356 (2012).
25. B. M. Reddy, P. Saikia and P. Bharali, *Catal. Surv. Asia*, **12**, 214 (2008).
26. S. Brunauer, P. H. Emmet and F. Teller, *J. Am. Chem. Soc.*, **60**, 309 (1938).
27. E. P. Barret, L. G. Joyner and P. P. Hanlenda, *J. Am. Chem. Soc.*, **73**, 373 (1951).
28. Y. He, X. Yu, T. Li, L. Yan and B. Yang, *Powder Technol.*, **166**, 72 (2006).
29. D. Sarkar, D. Mohapatra, S. Ray, S. Bhattacharyya, S. Adak and N. Mitra, *Ceram. Int.*, **33**, 1275 (2007).
30. P. R. Potti and V. C. Srivastava, *Ind. Eng. Chem. Res.*, **51**, 7948 (2012).
31. H. Cui, M. Zayat and D. Levy, *Chem. Mater.*, **17**, 5562 (2005).
32. L. Samiee, A. Beitollahi and A. Vinu, *Res. Chem. Intermed.*, **38**, 1467 (2012).
33. L. Samiee and A. Beitollahi, DOI:10.1007/s11164-013-1329-3.
34. K. S. W. Sing, D. H. Everett, R. A. W. Haul, L. Moscou, R. A. Pierotti, J. Rouquérol and T. Siemieniewska, *Pure Appl. Chem.*, **57**, 603 (1985).
35. J. Rouquérol, J. H. Avnir, C. W. Fairbridge, D. H. Everett, J. H. Haynes, N. Pernicone, J. D. F. Ramsay, K. S. W. Sing and K. K. Unger, *Pure Appl. Chem.*, **66**, 1739 (1994).
36. L. Samiee, F. Shoghi and A. Vinu, *Appl. Surf. Sci.*, **265**, 214 (2013).
37. M. Grun, A. A. Kurgabov, S. Schacht, F. Schuth and K. K. Unger, *J. Chromatogr. A.*, **740**, 1 (1996).
38. M. V. D. Borgmann and G. Wedler, *J. Catal.*, **212**, 10 (2002).
39. G. D. Halsey, *J. Chem. Phys.*, **16**, 931 (1948).
40. M. Sato, T. Sukegawa, T. Suzuki and K. Kaneko, *J. Phys. Chem. B.*, **101**, 1845 (1997).
41. K. Tanabe, M. Misono, Y. Ono and H. Hattori, *Stud. Surf. Sci. Catal.*, **51**, 5 (1989).
42. C. Murugan, H. C. Bajaj and R. V. Jasra, *Catal. Lett.*, **137**, 224 (2010).
43. P. Kumar, V. C. Srivastava and I. M. Mishra, *Catal. Commun.*, **60**, 27 (2015).
44. J. Xu, H. T. Wu, C. M. Ma, B. Xue, Y. X. Li and Y. Cao, *Appl. Catal. A: Gen.*, **464-465**, 357 (2013).
45. R. Juarez, A. Corma and H. Garcia, *Green Chem.*, **949–952**, 11 (2009).
46. L. Wang, Y. Wang, S. Liu, L. Lu, X. Ma and Y. Deng, *Catal. Commun.*, **45-49**, 16 (2011).
47. Z.-M. Cui, Z. Chen, C.-Y. Cao, W-G Song and L. Jiang, *Chem. Commun.*, **6093-6095**, 49 (2013).
48. J. Xu, K.-Z. Long, F. Wu, B. Xue, Y.-X. Li and Y. Cao, *Appl. Catal. A: Gen.*, **1-7**, 484 (2014).

Supporting Information

Dimethyl carbonate synthesis *via* transesterification of propylene carbonate with methanol by ceria-zinc catalysts: Role of catalyst support and reaction parameters

Praveen Kumar, Vimal Chandra Srivastava[†], and Indra Mani Mishra

Department of Chemical Engineering, Indian Institute of Technology Roorkee, Roorkee 247667, Uttarakhand, India

Table S1. Literature review on characterization of of ceria-zinc based catalysts for various applications

Characterization technique	Xie et al. [27] CeO_2-ZnO	Rajgure et al. [28] CeO_2-ZnO	Mi et al. [29] Ce-ZnF_2O_3	Joe et al. [22] ZnO (X)-CeO_2 (1-X)	Zhong et al. [30] $Ce_{1-x}Zn_xO_{2-\delta}$ oxide	Ying et al. [31] $Ce_{1-x}Zn_xO_y$	Wang et al. [32] $S_2O_8^{2-}/AL_x$ wt% Ce-Zn-O	Ma et al. [33] ZnO-eO_2	Mishra and Rao [34] CeO_2-ZnO	He et al. [35] CeO_2/ZnO	This work CeO_2-ZnO/support Al_2O_3/SiO_2/TiO_2
XRD	X	X	X	X	X	X	X	X	X	X	X
N2-sorption	X		X	X				X		X	X
SEM/EDS	X	X	X		X		X	X	X	X	X
FTIR	X						X				X
TPD-NH_3				X					X		X
TPD-CO_2				X						X	X
TEM	X	X			X			X			
CHNS									X		
TPD-methanol						X					
Process	CO oxidation	Gas sensor	Desulfurization	Urea methanolysis	CO Oxidation	Oxidative stem reforming	Esterification	Photocatalytic oxidation	Cyclohexanol dehydrogenation	Oxidative reaction of CO_2	Synthesis
End products	CO_2, H_2, H_2O			Dimethyl carbonate	CO_2, H_2, H_2O	Hydrogen	n-Butyl acetate			C_2 Hydrocarbons	Dimethyl carbonate

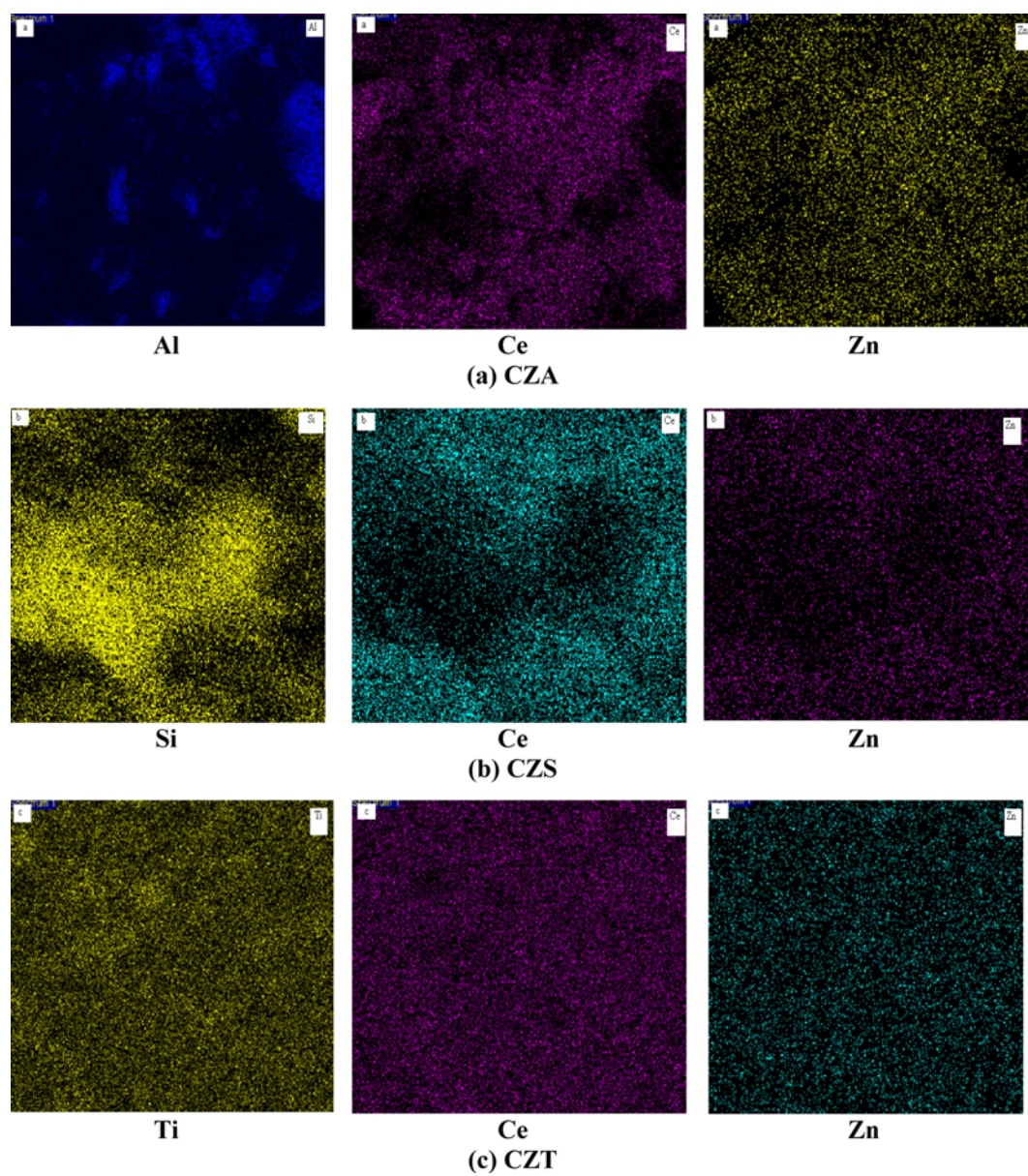X denotes that particular study reported in the study

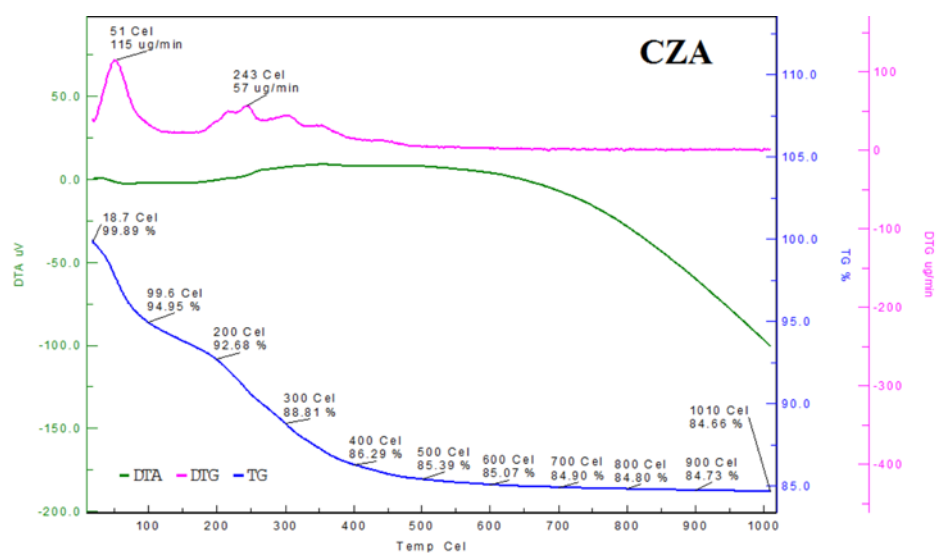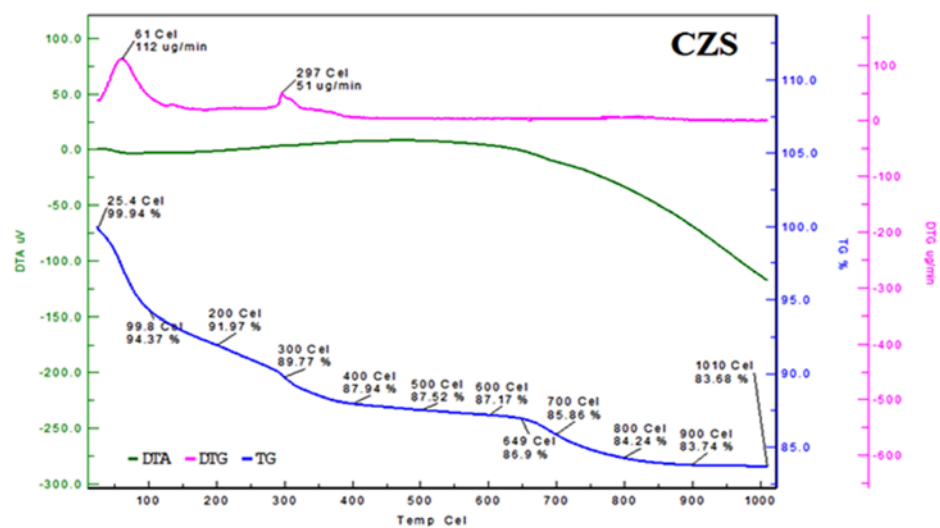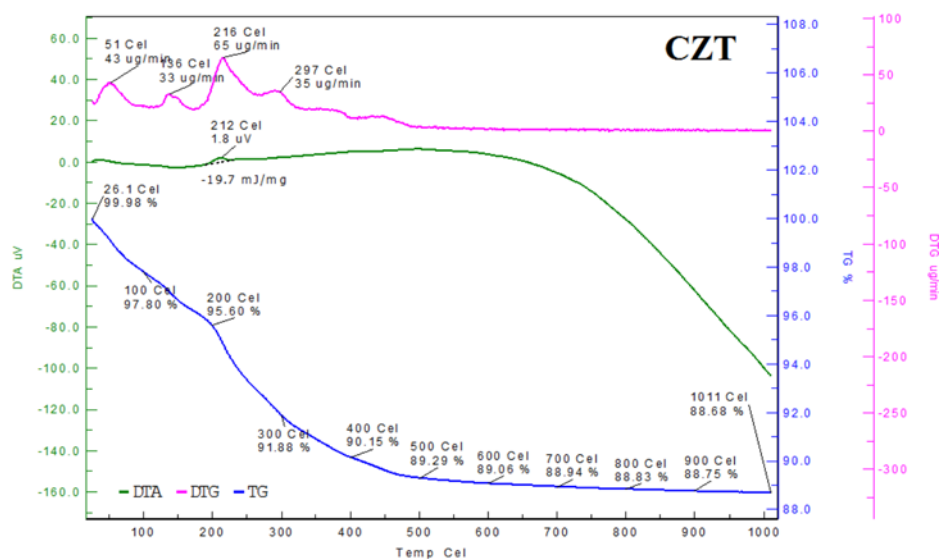**Fig. S1.** EDX image mapping of (a) Al, Ce, Zn element in CZA, (b) Si, Ce, Zn element in CZS, and (c) Ti, Ce, Zn element in CZT.

Fig. S2. TG/DTA/DTG of synthesized CZA, CZS and CZT catalysts.